The influence of the exposure conditions on the simulated photodegradation process of polyester-urethane coatings

Polymer Degradation and Stability 123 (2016) 121–130

Contents lists available at ScienceDirect

Polymer Degradation and Stability

journal homepage: www.elsevier.com/locate/polydegstab

The influence of the exposure conditions on the simulated photodegradation process of polyester-urethane coatings

Koen N.S. Adema [a, b], Hesam Makki [a, b], Elias A.J.F. Peters [a], Jozua Laven [a], Leendert G.J. van der Ven [a], Rolf A.T.M. van Benthem [a], Gijsbertus de With [a, *]

[a] Eindhoven University of Technology, Laboratory of Materials and Interface Chemistry, Department of Chemical Engineering and Chemistry, P.O. Box 513, 5600 MB, Eindhoven, The Netherlands
[b] Dutch Polymer Institute (DPI), P.O. Box 902, 5600 AX, Eindhoven, The Netherlands

ARTICLE INFO

Article history:
Received 23 September 2015
Received in revised form
2 November 2015
Accepted 16 November 2015
Available online 22 November 2015

Keywords:
Kinetic Monte Carlo
Simulation
Photodegradation
Polymer coating
Polyester-urethane

ABSTRACT

A kinetic Monte Carlo method to simulate photodegradation of a polymer coating is applied to the weathering process of a polyester-urethane clearcoat during artificial exposure under different conditions. Firstly, the optimised simulation parameters that yield the best match with experimentally measured results on the depth-resolved ester and urethane bond fractions are determined and compared for two different aerobic exposure experiments (one in a Weather-Ometer (WOM) and one in a Suntest equipment). Secondly, several other quantities that are obtained from the simulations, but cannot be determined experimentally, are compared, such as the fraction of newly formed crosslink bonds, absorptivity states, oxidised states, the fraction of radicals, the concentration of oxygen and the total amount of remaining material. Depth-inhomogeneity of the rate of photon absorption leads to the formation of distinct depth gradients in the WOM simulation, while a much more homogeneous evolution is obtained for the Suntest-air simulation. Photo-oxidative damage in the WOM simulation is more concentrated on the upper layer of the coating, resulting in the extensive evaporation of highly oxidised material, whereas degradation in the Suntest-air simulation is more spread out over the entire coating thickness, resulting in less material loss.

1. Introduction

One of the key questions that researchers in the field of polymer photodegradation try to answer is how the performance of a polymer application is influenced by the circumstances that the material is subjected to during its service life. In a previous publication [1] the influence of the conditions of different artificial exposure experiments on the photodegradation process of a model polyester-urethane clearcoat has been studied experimentally. Amongst other insights, this experimental study showed that the spectral power distribution and the type of atmosphere in which degradation occurs (aerobic or anaerobic) largely influence the depth-resolved evolution of the chemical composition of a degrading coating, in terms of both the type of degradation reactions ("degradation pathway") and the rates of these reactions at different coating depths ("depth-inhomogeneity").

In the present article a similar study is conducted, following the approach of coarse-grained computer simulations based on a kinetic Monte Carlo (KMC) method that has been introduced in previous work [2]. In that article, depth-resolved coating degradation was simulated by modelling the depth-dependency of physical processes that occur in the coating, such as the absorption of photons and the diffusion of oxygen, together with a procedure to simulate individual degradation reactions based on a rate-weighted KMC algorithm. By matching the simulated chemical depth gradients to their experimental counterparts, the numerical values of several kinetic and physical parameters, such as various reaction rate constants, can be obtained via this method.

The number of simulation studies in the field of polymer photodegradation, in which a similar attempt was made, is very limited. Among these few studies, three types of approaches can be distinguished if one considers the extent to which the specific chemistry of the degrading material is taken into account. Studies in which the chemistry is completely disregarded include earlier attempts to simulate changes in surface topography [3] and a

* Corresponding author.
E-mail address: G.deWith@tue.nl (G. de With).

http://dx.doi.org/10.1016/j.polymdegradstab.2015.11.014
0141-3910/

statistical approach [4,5]. Such a statistical approach to degradation is based on the notion that the time it takes for a coating to fail can differ dramatically in different climatological conditions. When a combination of climate and consumer/population distribution is taken into account, together with process variability during coating manufacture, the probability of failure can be assessed for any location with known climatological parameters [5]. The practical value of such an approach will be clear, but due to its generality, it is not very insightful for learning how degradation processes are influenced by specific factors causing degradation.

A second type of simulation approach involves a rather general consideration of the coating chemistry, without specification of the precise chemical structure and degradation mechanisms. Such an approach has been used for Monte Carlo simulations of coating degradation with a focus on the evolution of the surface topography and its relation to various physical characteristics [6,7]. The change of the coating chemistry during degradation was modelled as "hardening" or "sensitising", that is, a decreased or increased vulnerability of coating material near the location at which photon-induced damage occurred [6]. Besides this artificial incorporation of the chemistry, the influence of specific degradation factors on weathering was not considered.

The third type of approach involves a much more detailed specification of the coating chemistry. An early example of such a specific study was published by Martin, who developed a stochastic model to predict the degradation process of PMMA [8]. More recent examples deal with the photo-oxidative degradation of polypropylene [9] and epoxy-amine coatings with high and low glass transition temperatures [10,11]. These latter studies use a formalism of reaction rate equations based on the specific degradation chemistry and then simulate the evolution during exposure by solving a system of differential equations. In addition, physical processes such as light attenuation and mass transport of oxygen and water are included and the depth-dependence of degradation is taken into account as well. Our previous simulation work on polyester-urethane coatings also followed this last type of approach and includes, in addition to the KMC simulations already mentioned, Dissipative Particle Dynamics (DPD) simulations [12] and Molecular Dynamics (MD) simulations to determine physical properties of degraded networks after a fine-graining procedure [13].

In addition to studying the effect of the exposure conditions on quantities that have also been determined experimentally before [1,14], several quantities that can only be observed in the simulations will also be determined for the different exposure conditions. Although the simulated evolution of these quantities cannot be directly verified, some interesting insights into degradation processes and pathways can be obtained from such a study.

2. Modelling and simulation setup

2.1. Polyester-urethane model system

The material of study consists of the hydroxyl-functional polyester of isophthalic acid (IPA) and neopentylglycol (NPG) that is crosslinked with the trimer of hexamethyldiisocyanate (HDT). The chemical structure of the virgin polyester-urethane is represented by four types of coarse-grained beads (clusters of atoms which are grouped together into a single entity) [2]. The polyester part is composed of two bead types, that is, the IPA residue, denoted as "aromatic bead" and the NPG residue, called "aliphatic bead". The HDT crosslinker is also composed of two types of beads: the isocyanurate ring, or "crosslinker body" (one per crosslinker molecule), and the isocyanate residue tail, or "crosslinker arm" (three per crosslinker molecule). Two types of bonds interconnecting the beads are modelled explicitly: the urethane bond (connecting crosslinker arm and aliphatic bead) and the ester bond (connecting aliphatic bead and aromatic bead). These bonds can be broken as a consequence of photodegradation reactions. In addition, new bonds may form due to, for example, radical recombination reactions. These "new crosslinks" (interconnecting two aromatic beads or two aliphatic beads) are also modelled explicitly.

Different properties are assigned to individual beads by a numerical coding system that reflects the internal state of a bead [2]. This internal state may change as a consequence of photodegradation reactions. Some of the defined properties are relevant for all different bead types (for example, the number and type of connecting bonds, the number of radicals on the bead) whereas other properties are only relevant for a specific type (for example, the characteristic related to the absorption of UV photons is only relevant for the aromatic bead type). This specificity also determines in which reaction mechanisms a bead may or may not participate in order to simulate the evolution of the system with progressing degradation [2].

The introduction of a coarse-grained representation already leads to a significant reduction in the number of entities to handle during the simulation, but for a large simulated volume, further simplification is required. This simplification is achieved by converting the chemical network with topology into a compositional representation of the network, without topology. In short, this step involves discarding all the connections between beads in the coarse-grained network representation, so that it is no longer known which individual beads are mutually connected, but instead the number of beads with a certain connection type is tracked [2].

The direct output of the simulations is the depth-resolved time evolution of the (coarse-grained) chemical composition, that is, of the number of all the different beads with different internal states. All the other chemical and physical output that is discussed in the remainder of this article, can be derived from the direct output by post-simulation analyses.

2.2. Simulated exposure experiments

One set of simulations aimed at representing experimental exposure in a Ci65A Weather-Ometer, or WOM (Atlas MTS), equipped with xenon arc lamps and borosilicate inner and outer filters [14]. This WOM exposure experiment was performed at a black standard temperature (BST) of 65 °C and an irradiance of approximately 57 Wm^{-2} (300–400 nm), and with a total cycle time of 2 h, composed of a 102 min dry cycle at 40–60% relative humidity and an 18 min wet cycle with water spray. Since the effect of water is not explicitly incorporated into the degradation model used for the simulations, the (wet/dry) cycling is not taken into account in the simulation of WOM exposure. The results of these simulations have been published previously [2].

Two other sets of simulations aimed at representing experimental exposure in a Suntest XXL + (Atlas MTS), equipped with xenon arc lamps and Coated Quartz inner/Daylight outer filters [1]. Two custom made exposure cells were installed inside the Suntest to control atmospheric conditions during exposure. One cell was continuously purged with dry air ("air-exposed samples") and the other with dry nitrogen ("nitrogen-exposed samples"). Non-cyclic exposure was performed at an irradiance set to 48 ± 2 Wm^{-2} (300–400 nm) as measured by the sensors outside the exposure cells. The settings were determined in such a way that during stationary operation, the resulting BST as measured inside the exposure cells was approximately equal to 65 °C, which is equal to the BST from WOM exposure.

2.3. Modelling of photodegradation, photon absorption and oxygen diffusion

The (coarse-grained) modelling of polyester-urethane photodegradation reactions, the modelling of photon absorption by the coating and the modelling of oxygen diffusion inside the coating have all been described before [2]. Although the spectral dependence of photon absorption during Suntest exposure was modelled according to the same method as used for the simulation of WOM exposure, only a single wavelength regime, ranging from 294 to 334 nm, was defined for the simulation of Suntest exposure (this is discussed in more detail in section 3.1).

2.4. Simulation setup for suntest exposure

Simulations of degradation during Suntest exposure were performed using the methods described in a previous publication [2]. First, the total simulated volume, denoted as the "box", is constructed. In principle, this box represents a spatially inhomogeneous, 3-dimensional coating volume. The box is then divided into (N_x, N_y, N_z) smaller elements, termed "cells", whose centres are located at different positions (x, y, z) in the box. The cells serve as representative volume elements of the coating, implying that the conditions inside each individual cell are considered as spatially homogeneous [2]. Initially, each cell contains the virgin polyester-urethane composition, that is, in the coarse-grained representation as introduced in section 2.1. After initialisation of the box composition and the rates of all individual reactions that may occur, a previously described kinetic Monte Carlo algorithm is used to simulate the time evolution of the box during degradation [2].

Similar to what was done in our previous work, the simulations in this article were performed with a 1-dimensional box, that is, a single column of cells, as the focus of this work is on the depth-(in)homogeneity of photodegradation. The simulation box consisted of a column of 350 cells with fixed cell dimensions of $(17.4 \cdot 17.4 \cdot 100)$ nm^3. The sensitivity of simulation results to the variation in parameter values and the optimisation of the initially unknown parameter values were performed according to the methods that have been described before [2].

3. Results and discussion

3.1. Spectral dependence and optimised simulation parameters

For the simulation of coating degradation during WOM exposure, the spectral dependence of photon absorption was split into two regimes [2]: the short wavelengths (270–294 nm) and the long wavelengths (294–334 nm). The spectral power distribution (SPD) of the Suntest, however, is zero at the short wavelengths, as can be seen from Fig. 1, in which the SPD of the Suntest (inside the exposure cells) is shown together with the SPD of the Weather-Ometer and the Florida solar spectrum. For the simulation of coating degradation during exposure in the Suntest (for brevity, from now on denoted as "Suntest simulation"), the short wavelength regime is therefore discarded and a single wavelength regime, between 294 and 334 nm, is defined.

Because the SPD $(\Phi(\lambda))$ within this wavelength regime is different for Suntest exposure as compared to WOM exposure, the effective surface irradiance ϕ_{eff} and the absorption cross-section of the virgin coating σ_0 (as introduced in a before [2]) have to be recalculated. Their resulting values are reported in Table 1.

After updating these optical parameters, a simulation was performed in which the remaining parameter values equal the values obtained from optimisation of the WOM simulation [2], that is, the optimised parameter set which will be denoted as $[P_{\text{WOM}}]$. Similar to the methodology in our previous work [2], the resulting simulated evolution of ester and urethane bond gradients was compared to the experimental counterparts obtained from infrared microscopy for Suntest-air exposure [1].

The resulting match was fair, but did not yet seem optimal, especially for the simulated urethane bond gradients, which were insufficiently steep. Therefore, a sensitivity analysis was performed for the Suntest-air simulation as well, similar to what was done for the WOM simulation [2]. The resulting response plots (shown in Supporting Information 1) look similar to those from the WOM simulation, with the main difference that one rate constant ($k_{\text{eva\_ali}}$) that still had medium-influence for the WOM simulation, does no longer significantly influence the ester and urethane bond results for the Suntest-air simulation. As a consequence, this parameter was excluded from the Jacobian that was used to optimise the Suntest-air simulation parameters. The resulting optimised parameter set $[P_{\text{Sun}}]$ is reported in Table 2.

In the last column of Table 2, the relative differences between the parameter values from $[P_{\text{WOM}}]$ and $[P_{\text{Sun}}]$ are reported. These differences are limited to only a few percent for most parameters with one exception: the oxygen diffusion coefficient for the Suntest-air simulation is about half as large as in the case of the WOM simulation. The explanation for this difference is most likely related to the presence of water in the coatings during WOM exposure, while the coatings are dry during Suntest exposure. The diffusion coefficient obtained for the Suntest-air simulation is therefore probably a better representation of the intrinsic diffusion coefficient value, whereas the WOM simulation represents oxygen diffusion through a coating that is plasticised by water.

3.2. Simulation of coating degradation during suntest exposure

The degradation of coatings during Suntest-air exposure was simulated by performing KMC simulations using $[P_{\text{Sun}}]$ with a stack of 350 cells, which corresponds to a coating thickness of 35 μm. The experimental and simulated depth-resolved evolutions of the remaining fraction of ester bonds and urethane bonds are shown in Fig. 2.

The experimental data shown in these graphs were obtained previously from infrared microscopy measurements [1]. In short, this method first requires the introduction of a depth profile in each coating sample by manually abrading the coating via a sandpaper treatment. The result of the sanding is that a new surface is formed, which consists of coating material that originates from different depths inside the coating before the treatment. An FTIR-ATR line scan is then performed along this depth profile in order to characterise the chemical composition of as a function of the lateral coordinate along the line (x). Finally, the depth profile $z(x)$ is determined from optical profilometry and the depth-resolved chemical composition can be obtained (details of the complete procedure can be found in a previous publication [14]).

The bulk levels of the simulated ester bond fraction (Fig. 2a) match well with the experimental results, but the bending towards a slightly lower concentration near the surface does not follow that well from the simulation (the inset in Fig. 2a). The difference is the largest for the late stages of degradation and is most likely caused by the fact that at this low dose rate condition, a significant fraction of the ester bonds is broken as a consequence of progressive oxidation of the aliphatic moieties they are connected to. In the simulation, however, the breakage of ester bonds was modelled as a purely photolytic process, which explains why the simulated rate of ester bond breakage at the surface lags a bit behind compared to the experimental one.

The overall match between experiment and simulation for the remaining fraction of urethane bonds (Fig. 2b) is quite good and the

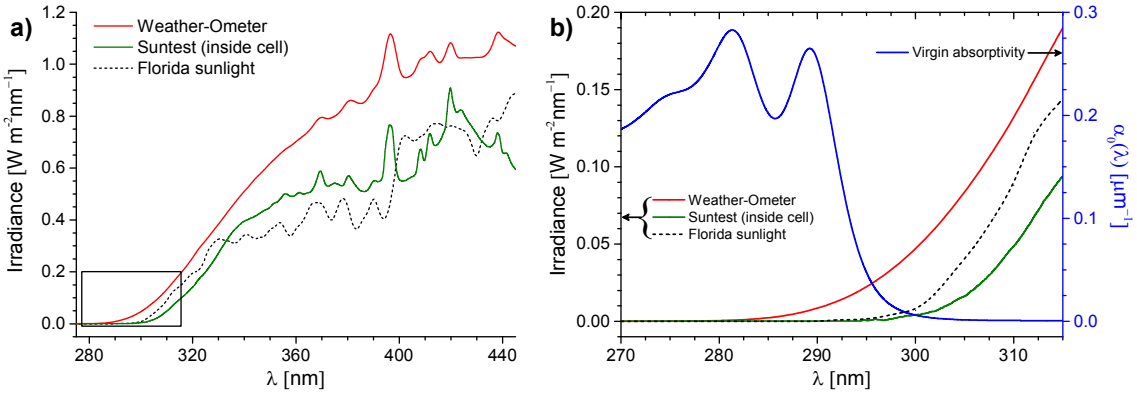

Fig. 1. Spectral power distributions of the Weather-Ometer (red), Suntest (green) and Florida sunlight (black). In Fig. 1b, a magnification of the SPD's inside the black rectangle of Fig. 1a is shown, together with the virgin coating absorptivity spectrum (blue line, right vertical axis). Graphs originate from previous work [1]. (For interpretation of the references to colour in this figure legend, the reader is referred to the web version of this article.)

Table 1
Fixed simulation parameters used for the Suntest simulations.

Parameter name	Symbol	Value	Unit	Calculated from
Irradiance	ϕ_{eff}	$2.580 \cdot 10^{22}$	$m^{-2}h^{-1}$	$\int_{294\ nm}^{334\ nm} d\lambda\ \Phi(\lambda)$
AbsCrossSec0	$\sigma_{0,eff}$	$7.398 \cdot 10^{-25}$	m^2	$\frac{1}{\rho_0} \frac{\int_{294\ nm}^{334\ nm} d\lambda\ \Phi(\lambda)\alpha_0(\lambda)}{\int_{294\ nm}^{334\ nm} d\lambda\ \Phi(\lambda)}$

main discrepancy is once again the steepness of the urethane bond gradients in the upper ≈10 μm of the coating, which was also the case for the simulation of WOM degradation [2]. The reason for this discrepancy remains unclear.

The degradation of coatings during Suntest-nitrogen exposure was also simulated using [P_{Sun}], with the only difference that the

Table 2
Optimised variable parameter set [P_{Sun}] used for the Suntest-air simulation.

Parameter name	Symbol	Value [Unit]	Diff. [P_{Sun}]:[P_{WOM}] [%]
Primary rate constants			
K_oxidation	k_{ox}	$1.557 \cdot 10^{-3}$ [h^{-1}]	−2.3
K_sink_ali	k_{sink_ali}	$1.023 \cdot 10^{-3}$ [h^{-1}]	+0.9
K_abstraction-H_ali	k_{absH_ali}	$0.763 \cdot 10^{-29}$ [m^3h^{-1}]	+0.7
K_abstraction-H_xl	k_{absH_xl}	$0.826 \cdot 10^{-29}$ [m^3h^{-1}]	−4.5
K_grafting	k_{graft}	$2.547 \cdot 10^{-29}$ [m^3h^{-1}]	−0.01
K_recombination_ali	k_{rec_ali}	$2.123 \cdot 10^{-29}$ [m^3h^{-1}]	+0.9
Secondary rate constants			
K_evaporation_ali	k_{eva_ali}	$1.020 \cdot 10^{-3}$ [h^{-1}]	–
K_evaporation_xl	k_{eva_xl}	$1 \cdot 10^{-3}$ [h^{-1}]	–
K_leaching	k_{leach}	$1 \cdot 10^{-3}$ [h^{-1}]	–
K_sink_aro	k_{sink_aro}	$1 \cdot 10^{-3}$ [h^{-1}]	–
K_recombination_aro	k_{rec_aro}	$2 \cdot 10^{-29}$ [m^3h^{-1}]	–
Other parameters			
AbsEnh(1/0)_L	$\sigma_{1,eff\_L}/\sigma_{0,eff\_L}$	11.8 [−]	−1.7
QuantumEff_sci	q	$0.721 \cdot 10^{-3}$ [−]	−4.0
DiffCoeff_oxygen	D_{O_2}	$2.01 \cdot 10^{-10}$ [m^2h^{-1}]	−54
SatConc_oxygen	$C_{O_2,sat}$	0.986 [mol m^{-3}]	−1.7

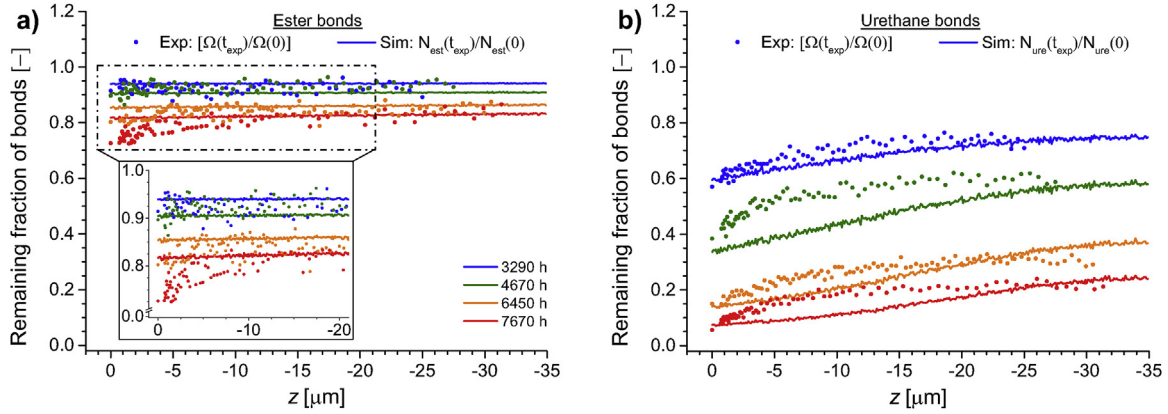

Fig. 2. Comparison between depth-resolved experimental (circles) and simulation results (lines) for Suntest-air exposure for a) ester bonds and b) urethane bonds. Different colours represent different exposure times.

oxygen saturation concentration was reduced. A numerical optimisation was not performed for this exposure condition because of the limited extent of degradation that could be achieved experimentally. From trial and error, it was observed that a reduction of $C_{O_2,sat}$ to about 8% of its value from [P_{Sun}] (corresponding to an oxygen concentration of approximately 1.5 v%) leads to a reasonable simulation of the experimental results for the ester and urethane bond gradients. These results are available in Supporting Information 2. The value obtained for the oxygen saturation concentration is quite a bit higher than what is expected for the amount of oxygen present in the nitrogen supply (typically, a few vpm). This higher value could be related to the fact that the experimentally studied coatings have been in contact with ambient air on several occasions during the period they have been exposed (e.g., after opening the cells and during the weighing of the panels at each sampled exposure time). Reactions with oxygen during this contact time could contribute to the high effective value of $C_{O_2,sat}$ that was obtained here. Next to that, the possibility that the degradation of urethane bonds follows a different pathway under anaerobic conditions, as suggested previously [1], could also provide an explanation. After all, if the availability of oxygen is not determining the rate of urethane bond breakage, one cannot expect that a simulation with an oxidative degradation mechanism for the urethane bonds can result into a good estimate of the experimental oxygen saturation concentration.

3.3. Other depth-resolved quantities obtained from simulations

Due to the complexity of polyester-urethane degradation, the influence of the exposure conditions on the chemical composition can only be studied to a limited extent by experimental methods (in this work, most notably via the ester and urethane bond depth gradients). The different degradation simulations, however, also provide information on many other interesting quantities, which are not easily accessed with experimental methods, or cannot be determined experimentally at all. These quantities include the fraction of new crosslink bonds (as compared to the total number of bonds), absorptivity states, oxidised states, the fraction of radicals, the concentration of oxygen and the total amount of remaining material. The simulation approach thus has the additional advantage that, next to experimentally accessible quantities like the ester and urethane bond fractions, it also yields predictions for several other quantities of interest.

In the following figures, the depth-resolved evolution of several quantities that result from the WOM simulation (left column of the figures) and the Suntest-air simulation (right column of the figures) is shown. The data for both WOM and Suntest-air exposure are plotted with the same scales to facilitate comparison and the same colours correspond to the same exposure times (the WOM simulation is analysed up to 4000 h, the Suntest-air simulation up to 8000 h). Quantities related to the bonds in the simulation box (Fig. 3), the beads in the box (Fig. 4) and the radical fraction and oxygen concentration in the box (Fig. 5) are reported. Details about the modelling of the degradation chemistry can be found in our previous work on degradation simulations [2].

From Fig. 3, the effect of (in)homogeneous photon absorption and oxygen concentration gradients can be clearly recognised for all three types of bonds. Although for individual bond types, substantial differences in the remaining bond fractions were found between both aerobic exposure conditions, the difference for the total remaining fraction of bonds (shown in Fig. 3d/D) is relatively small. The differences in rates are obvious as well. Difference in depth-homogeneity is also clear from a number of bead-related quantities as plotted in Fig. 4. Not very surprisingly, the gradients in the fraction of aromatic beads with an increased absorptivity (Fig. 4a/A) show much similarity with the gradients in the fraction of newly formed crosslinks (Fig. 3c/C).

Fig. 4b/B and c/C show information about the occurrence of beads in the first and second oxidised states, respectively. The definition of bead oxidation states in the simulation scheme is based on the presence of sites in the polymer structure that are most prone to oxidation due to the presence of labile hydrogen atoms that are easily abstracted. These labile hydrogen atoms occur predominantly at the carbon atoms in the α-positions to the ester and urethane bonds in the coating [15–17]. In other words, the definition of bead oxidation states is thus based on the occurrence of ester and urethane bonds in the polymer structure. For this reason, it was modelled that an aliphatic bead can be oxidised two times at most (as it is initially connected by two ester bonds or by one ester bond and one urethane bond) and that a crosslinker arm bead can only be oxidised once (as it is initially connected by one urethane bond). Naturally, this model strongly simplifies the complicated oxidation pathways that one expects to exist in reality.

Part of the material loss during degradation is modelled by the evaporation mechanisms (details can be found in a previous publication [2]), which allow a maximally oxidised bead to escape the simulation box at a certain rate. As a consequence of the definition of bead oxidation states, aliphatic beads in their second oxidised state are thus considered as (metastable) volatiles, whereas their first oxidised state is considered as a (stable) non-volatile species. For crosslinker arm beads, their first oxidised state is also their maximally oxidised state and hence they may evaporate after undergoing only a single oxidation event. For both exposure conditions, the gradient of the first oxidation state (shown in Fig. 4b/B) initially develops as a monotonic, convex shape, but changes into an S-shaped curve at later exposure times. This observation will be discussed in more detail in the next section. Aliphatic beads in the second oxidised state (Fig. 4c/C) are only present in significant amounts during the later stages of degradation ($\geq$ 1500 h for WOM simulation, $\geq$ 4000 h for Suntest-air simulation) and only in the upper 6–10 μm of the box, where the oxygen concentration is the highest.

For the Suntest-air simulation, the total remaining fraction of beads develops similarly to the total remaining fraction of bonds (Figs. 4 and 3D), but for the WOM simulation, there is quite a difference between the evolution of these two quantities. At the later stages of WOM degradation, the bond loss rate near the surface slows down much more than the bead loss rate, leading to a depth gradient of the remaining bead fraction that is larger than that of the remaining bond fraction. Also this observation will be revisited in the next section.

Finally, the fraction of beads carrying a radical and the oxygen concentration gradients are shown in Fig. 5a/A and Fig. 5b/B, respectively. During the intermediate stages, the radical fraction in the WOM simulation is about twice as large as in the Suntest-air simulation. For both simulations, a difference in the shapes of the radical gradients can be seen between the early stage and the late stage of degradation. The oxygen concentration profiles for both conditions look quite similar after the initial development, although the stationary bulk level in the WOM simulation is approximately 0.08 mol m^{-3} lower in comparison with the Suntest-air simulation.

Plots, similar to those shown in Figs. 3–5 were obtained for the simulation of Suntest-nitrogen exposure. For most of these quantities, the evolution during the Suntest-nitrogen simulation looks very similar to the evolution during Suntest-air exposure, but at lower rates. The most notable differences are obviously observed for the quantities most closely related to oxidation (for example, much lower rates of urethane bond breakage and the formation of

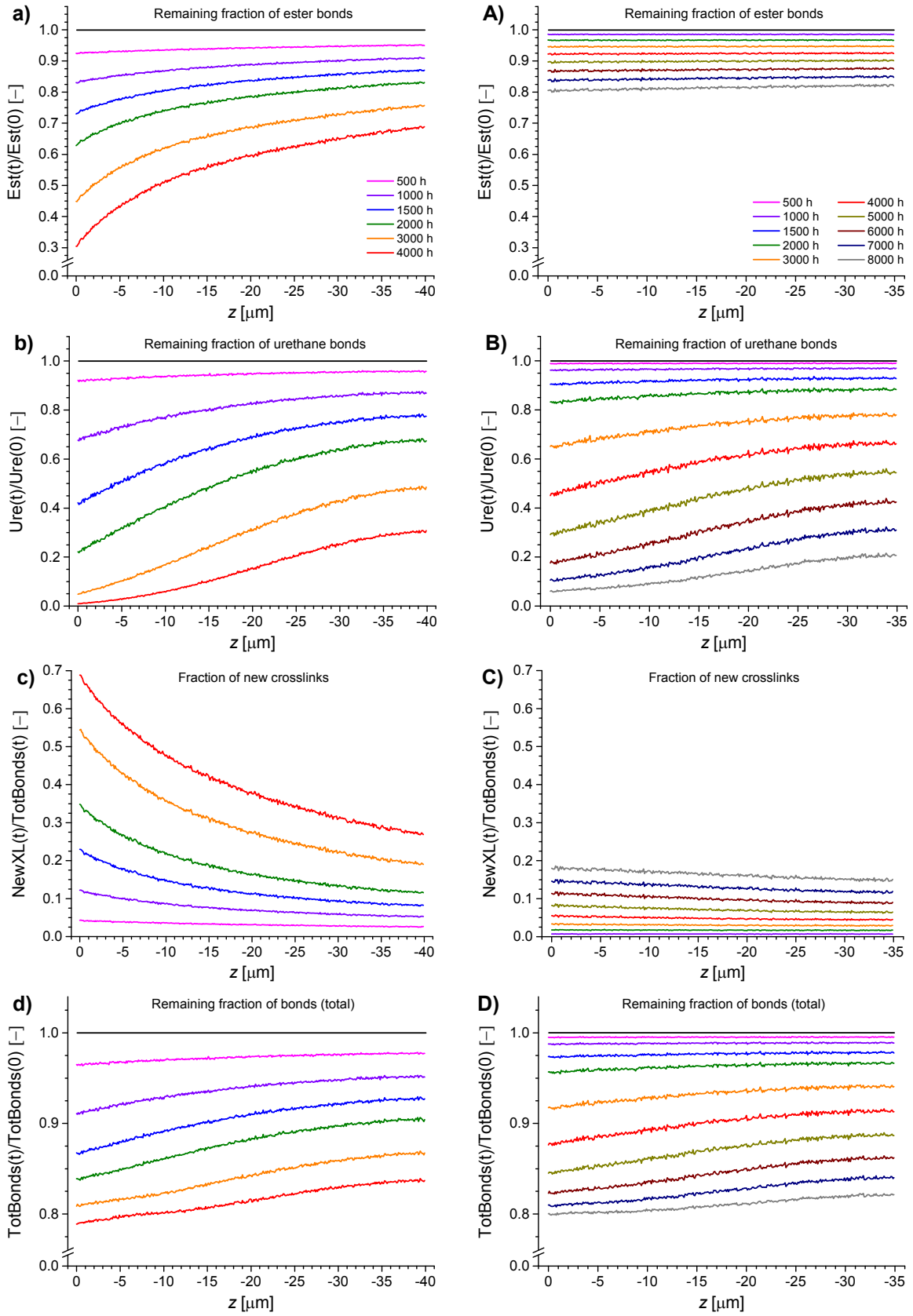

Fig. 3. Simulated depth-dependent evolution of chemical bonds at regular time intervals for WOM exposure (a–d, left column) and Suntest-air exposure (A–D, right column), for the fraction of ester bonds (a/A), urethane bonds (b/B), new crosslinks (c/C) and the total remaining fraction of bonds (d/D).

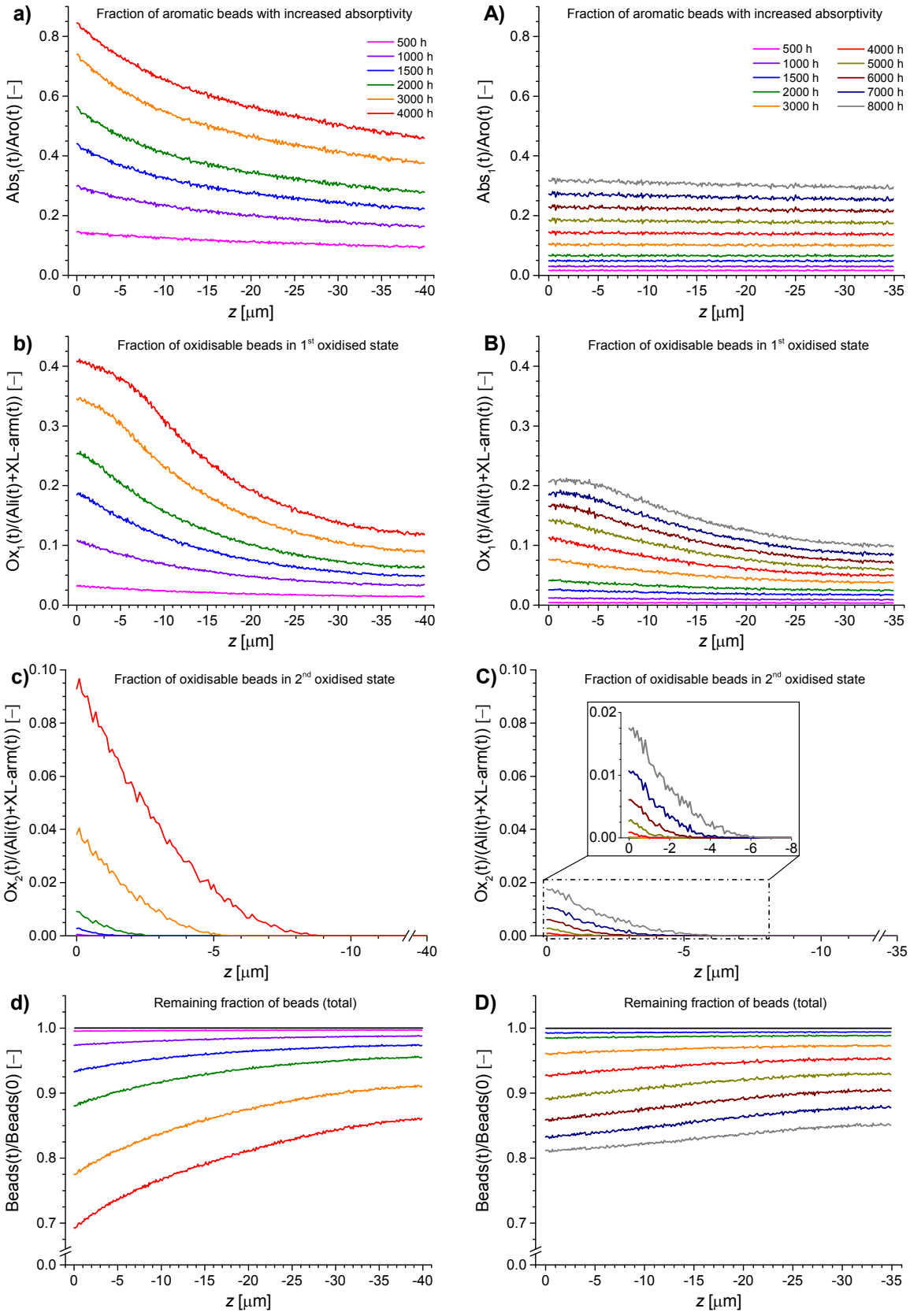

Fig. 4. Simulated depth-dependent evolution of beads at regular time intervals for WOM exposure (a–d, left column) and Suntest-air exposure (A–D, right column), for the (aromatic) beads with increased absorptivity (a/A), the 1st oxidised state (b/B), the 2nd oxidised state (c/C) and the total remaining fraction of beads (d/D).

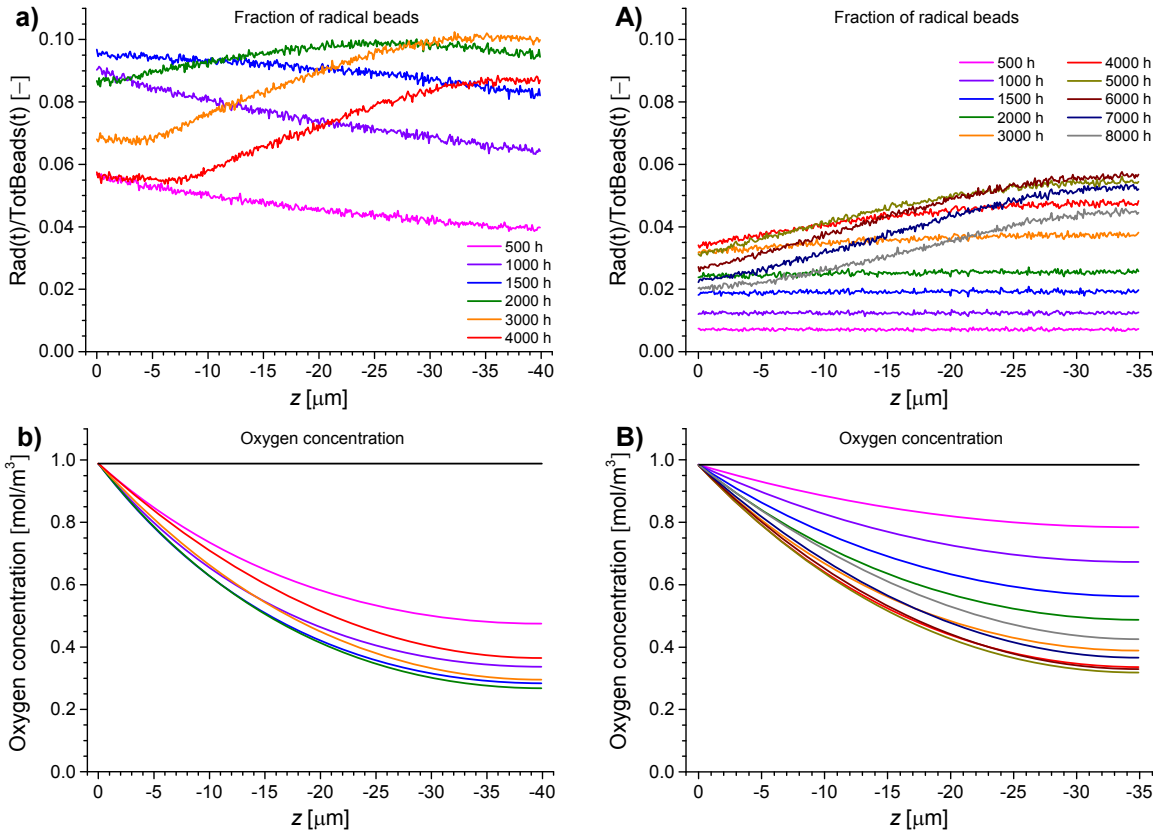

Fig. 5. Simulated evolution of depth gradients at regular time intervals for WOM exposure (a–b, left column) and Suntest-air exposure (A–B, right column), for the fraction of radical beads (a/A) and the concentration of oxygen (b/B).

the first oxidised state, the second oxidised state remains absent after even 8000 h). Also the radical bead fraction evolves rather differently in the Suntest-nitrogen case, as it keeps growing continuously and reaches a higher level as compared to the Suntest-air case (after 8000 h, a radical bead fraction of about 13% is reached, as compared to a maximal value of approximately 6% for the Suntest-air simulation).

3.4. Time-resolved evolution of the upper layer during simulation

In the previous section, the depth-resolved simulation results for only a few selected exposure times were presented. In addition to such a visualisation of the simulation outcome, it is also insightful to study the fully time-resolved results for a part of the box at a certain depth. In Fig. 6, such a time-resolved visualisation is shown for the upper 1 μm of the simulation box for both the WOM simulation (left column) and the Suntest-air simulation (right column). Please, note that the time scales (horizontal axes) are different for the two conditions.

In Fig. 6a/A, the bond composition in the upper 1 μm of the box is shown. In a late stage of the WOM simulation, the total remaining fraction of bonds mainly consists of newly formed crosslinks, whereas in the Suntest-air simulation, the ester bonds remain the predominant bond type. In both conditions, the newly formed crosslinks mainly consist of aromatic crosslinks, with a ratio of about 2 aromatic crosslinks for every 1 aliphatic crosslink at long exposure time.

The fraction of oxidisable beads is shown for the aliphatic beads (Fig. 6b/B) and for the crosslinker arm beads (Fig. 6c/C). In the WOM simulation, a much larger fraction of the non-oxidised aliphatic beads (blue lines in Fig. 6b/B) is converted into an oxidised species and more aliphatic beads are removed from the box (black lines) as compared to the Suntest-air simulation. This larger removal rate of aliphatic beads is also the cause of the larger ratio [bead loss rate/bond loss rate] that was observed for WOM exposure (Fig. 3d and Fig. 4d). The fraction of oxidised crosslinker arm beads (orange lines in Fig. 6c/C) shows a clear maximum in both simulations. On the right side of this maximum, the rate of disappearance of these beads (by evaporation) exceeds their rate of formation (by oxidation). This same condition, which mainly occurs close to the surface where the oxidation rates are the highest, is also responsible for the transition from a convex shape to an S-shaped curve in the depth-resolved plots in Fig. 4c/C.

Finally, the radical bead fractions are shown in Fig. 6d/D (please, note that the vertical scaling is different). The aromatic radical fraction remains very low throughout the simulations and the crosslinker arm radical fraction shows similarity with the fraction of its first oxidised state (Fig. 4c/C), as can be expected from their mechanistic relation.

4. Conclusions

The kinetic Monte Carlo method to simulate the photodegradation process of a polyester-urethane coating, as introduced in a previous publication [2], has been applied to simulate degradation during Suntest exposure, with the aim of studying the influence of the exposure conditions on the simulated degradation process. For this purpose, the spectral dependence of photon absorption has been remodelled to account for the fact that the irradiance spectrum of Suntest exposure has zero intensity at the

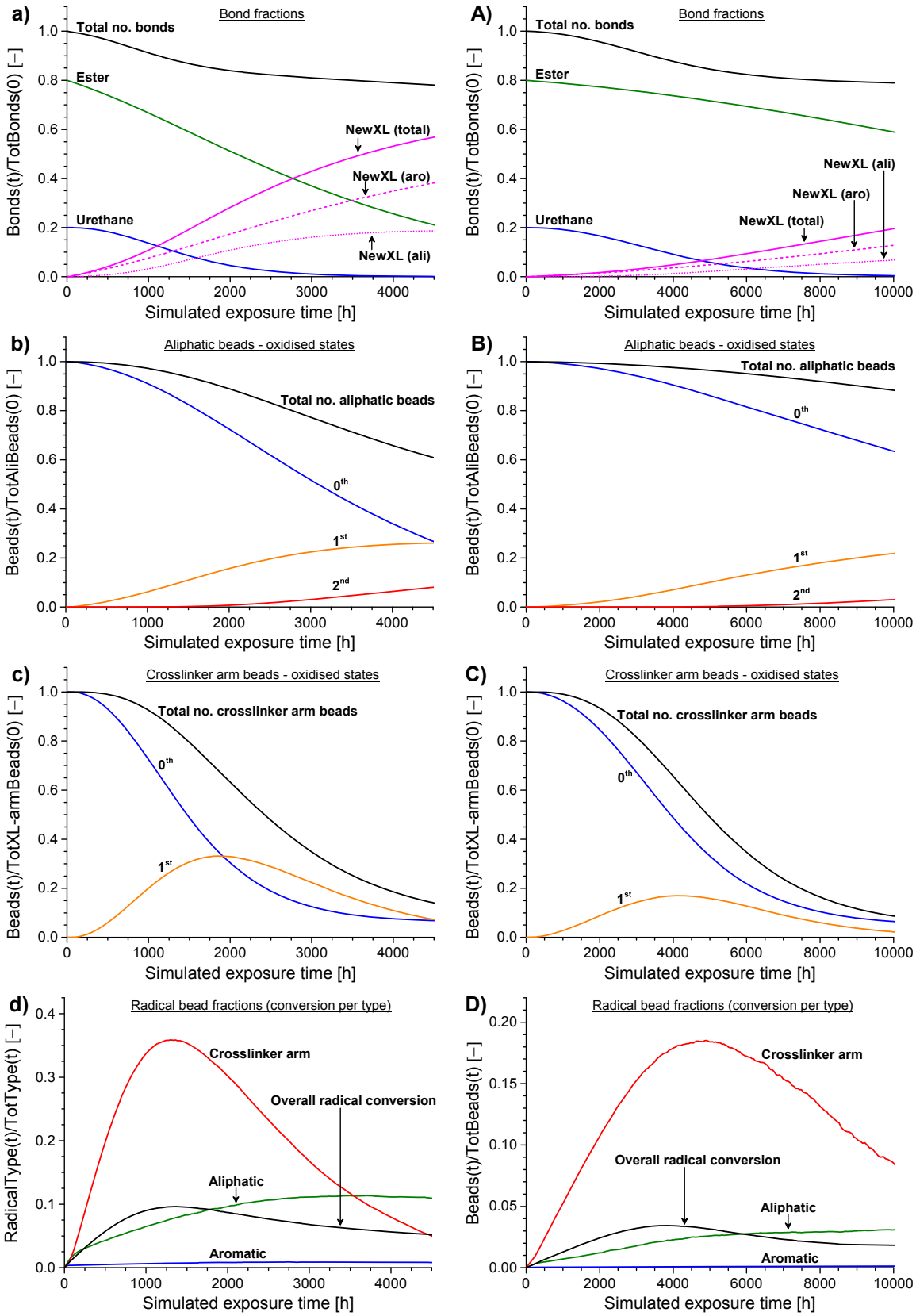

Fig. 6. Simulated time evolution of the upper 1 μm of the simulation box of WOM exposure (a–d, left column) and Suntest-air exposure (A–D, right column), for the bond fractions (a/A), the aliphatic beads (b/B), the crosslinker arm beads (c/C) and the radical beads (d/D).

short wavelengths with associated low penetration depths, whereas these wavelengths have nonzero intensity in the spectral

power distribution of the Weather-Ometer. A sensitivity analysis was performed for the parameters of the Suntest-air simulation and an optimised parameter set [P_{Sun}] for the degradation process involved, was obtained. This parameter set [P_{Sun}] resembles well the optimised parameter set that was obtained for the WOM simulation ([P_{WOM}]) [2], with the exception that the oxygen diffusion coefficient in [P_{Sun}] is about half as large as in [P_{WOM}]. This difference is attributed to plasticisation of the coating due to the presence of water during WOM exposure.

The simulated depth gradients of the remaining fraction of ester bonds showed a good overall match with the experimental data, which indicates that the modelled description of photon absorption results in a proper description of depth-resolved photolysis. The rate of ester bond breakage close to the surface was slightly underestimated in the later stages of degradation, which is attributed to the fact that due to the low dose rate during Suntest exposure, a significant fraction of the ester bonds is broken via a photo-oxidative pathway rather than via a purely photolytic one. For the remaining fraction of urethane bonds, the match between experimental and simulated depth gradients was quite good. The main discrepancy is the steepness of the gradients in the upper ≈ 10 μm of the coating, which has also been observed for the WOM simulation [2].

In addition to the evolution of the ester and urethane bond fractions, also a number of other quantities that characterise the composition of the coating and which cannot be determined experimentally, have been studied and a comparison was made between WOM and Suntest-air degradation. Depth-inhomogeneity of the rate of photon absorption leads, for WOM, to the formation of distinct depth gradients for the fraction of new crosslinks, the absorptivity increase, the fraction of oxidised beads and the total remaining fraction of beads, while a much more homogeneous evolution of these quantities is obtained for the Suntest-air simulation. Highly oxidised species, in the degradation model represented by aliphatic beads in their second oxidised state, are only present in significant amounts in the later stages of degradation in the upper 6–10 μm of the coating, due to the high concentration of oxygen in this layer. During the later stages of degradation in the WOM, the relative decrease of the total fraction of beads is faster than that of the total fraction of bonds, whereas in the Suntest-air simulation, these rates of decrease are similar. In other words, the loss of material in the WOM simulation is larger than in the Suntest-air simulation, whereas the total number of bonds is similar (although the bond composition is rather different). This difference indicates that WOM degradation can be considered as more localised (progressive damage is largely concentrated on the material in the upper layer of the coating, leading to the loss of highly oxidised material) than Suntest-air degradation, which is more spread out over the entire coating thickness.

A fully time-resolved visualisation of the evolution in the upper 1 μm of the simulation box provided additional insight into the relations between compositional quantities. In a late stage of the WOM simulation, the total remaining fraction of bonds is mainly composed of newly formed crosslinks, whereas in the Suntest-air simulation, the ester bonds remain the major component. Approximately twice as many aromatic crosslinks than aliphatic crosslinks are observed in both simulations. In the WOM simulation, a much larger fraction of the initially non-oxidised aliphatic beads is converted into an oxidised species, which is also in agreement with the larger amount of material loss. In both simulations, the fraction of crosslinker arm beads in the oxidised state shows a maximum during the intermediate stage of degradation, which results from a shift in the balance between formation (via oxidation) and disappearance (via evaporation) during the simulation.

The simulation results obtained in this chapter lead to a significantly more detailed insight into how the composition of a coating changes during exposure and they help to better understand the nature of the photodegradation process in relation to the exposure conditions. In addition, the observation that a single simulation method, implemented with a single set of parameter values, is able to predict the photodegradation process that takes place during two quite different (aerobic) exposure experiments, promises a good perspective for the application in service life prediction studies.

Acknowledgements

This research forms part of the research programme of the Dutch Polymer Institute (DPI), project #713.

Appendix A. Supplementary data

Supplementary data related to this article can be found at http://dx.doi.org/10.1016/j.polymdegradstab.2015.11.014.

References

[1] K.N.S. Adema, H. Makki, E.A.J.F. Peters, J. Laven, L.G.J. van der Ven, R.A.T.M. van Benthem, G. de With, The influence of the exposure conditions on the chemical and physical changes of polyester-urethane coatings during photodegradation, Polym. Degrad. Stab. 123 (2016) 13–25.
[2] K.N.S. Adema, H. Makki, E.A.J.F. Peters, J. Laven, L.G.J. van der Ven, R.A.T.M. van Benthem, G. de With, Kinetic Monte Carlo simulation of the photodegradation process of polyester-urethane coatings, Phys. Chem. Chem. Phys. 17 (2015) 19962–19976.
[3] F.Y. Hunt, M.A. Galler, J.W. Martin, Microstructure of weathered paint and its relation to gloss loss: computer simulation and modeling, J. Coat. Technol. 70 (1998) 45–53.
[4] D.R. Bauer, Predicting in-service weatherability of automotive coatings: a new approach, J. Coat. Technol. 69 (1997) 85–96.
[5] M.E. Nichols, J.F. Frey, Statistical modeling of coating lifetimes in disparate environments, J. Coat. Technol. Res. 12 (2015) 49–61.
[6] B. Hinderliter, S.G. Croll, Monte Carlo approach to estimating the photodegradation of polymer coatings, JCT Res. 2 (2005) 483–491.
[7] B.R. Hinderliter, S.G. Croll, Simulations of nanoscale and macroscopic property changes on coatings with weathering, JCT Res. 3 (2006) 203–212.
[8] J.W.A. Martin, Stochastic model for predicting the service life of photolytically degraded poly(methyl methacrylate) films, J. Appl. Polym. Sci. 29 (1984) 777–794.
[9] A. François-Heude, E. Richaud, E. Desnoux, X. Colin, A general kinetic model for the photothermal oxidation of polypropylene, J. Photochem. Photobiol. A Chem. 296 (2015) 48–65.
[10] S. Kiil, Model-based analysis of photoinitiated coating degradation under artificial exposure conditions, J. Coat. Technol. Res. 9 (2012) 375–398.
[11] S. Kiil, Mathematical modeling of photoinitiated coating degradation: effects of coating glass transition temperature and light stabilizers, Prog. Org. Coat. 76 (2013) 1730–1737.
[12] H. Makki, K.N.S. Adema, E.A.J.F. Peters, J. Laven, L.G.J. van der Ven, R.A.T.M. van Benthem, G. de With, A simulation approach to study photo-degradation processes of polymeric coatings, Polym. Degrad. Stab. 105 (2014) 68–79.
[13] H. Makki, Modeling and Physical Study of Weathering of a Polyester-urethane Coating, PhD thesis, Eindhoven University of Technology, 2015.
[14] K.N.S. Adema, H. Makki, E.A.J.F. Peters, J. Laven, L.G.J. van der Ven, R.A.T.M. van Benthem, G. de With, Depth-resolved infrared microscopy and UV-VIS spectroscopy analysis of an artificially degraded polyester-urethane clearcoat, Polym. Degrad. Stab. 110 (2014) 422–434.
[15] P. Malanowski, S. Huijser, F. Scaltro, R.A.T.M. van Benthem, L.G.J. van der Ven, J. Laven, G. de With, Molecular mechanism of photolysis and photooxidation of poly(neopentyl isophthalate), Polymer 50 (2009) 1358–1368.
[16] P. Malanowski, R.A.T.M. van Benthem, L.G.J. van der Ven, J. Laven, S. Kisin, G. de With, Photo-degradation of poly(neopentyl isophthalate). part II: mechanism of cross-linking, Polym. Degrad. Stab. 96 (2011) 1141–1148.
[17] C. Wilhelm, J.-L. Gardette, Infrared analysis of the photochemical behaviour of segmented polyurethanes. 1. aliphatic poly(ester-urethane), Polymer 38 (1997) 4019–4031.